

Mechanism of Acetylene–Vinylidene Rearrangement with Na, Al, and Y Atoms

Eric D. Glendening* and Matthew L. Strange

Department of Chemistry, Indiana State University, Terre Haute, Indiana 47809

Received: January 10, 2002; In Final Form: May 31, 2002

Reaction pathways are identified for Na-, Al-, and Y-induced acetylene (HCCH)–vinylidene (CCH₂) rearrangements in the gas phase. Density functional and coupled cluster calculations are performed with basis set extrapolations. The rearrangement barriers decrease from 44.0 kcal/mol in the metal-free reaction to 41.3 (Na), 19.1 (Al), and 16.1 (Y) kcal/mol in the metal-induced reactions. This decrease results from the strengthening of the M–C bonds (Na–C < Al–C < Y–C) in the M(HCCH) and M(CCH₂) complexes. Natural bond orbital analysis reveals the metallacyclopropene and metallallene character of several of the M(HCCH) and M(CCH₂) complexes. In addition, analysis of the transition states provides a detailed picture of the redistribution of bonding and nonbonding electrons along the reaction pathway. The metal-free and Na-induced rearrangements proceed via 1,2-hydride shifts, whereas the Al- and Y-induced reactions proceed via 1,2-hydrogen shifts. The latter reactions involve homolytic bond cleavage and formation, with the α and β electron densities undergoing redistribution in opposing directions.

Introduction

Vinylidene (:C=CH₂) is an electron-deficient and highly unstable isomer of acetylene (HC≡CH). Theoretical investigations^{1–4} have established that gas-phase vinylidene is approximately 43 kcal/mol less stable than acetylene and that the barrier for HCCH → CCH₂ isomerization is ca. 44–45 kcal/mol. Thus, there exists only a 1–2 kcal/mol barrier preventing vinylidene from rearranging to acetylene. Although vinylidene is unstable in the gas phase, it is strongly stabilized through complexation to metal atoms (M).⁵ Indeed, several metal–vinylidene complexes have been identified that are more stable than their acetylene isomers.^{6–8}

The mechanisms for metal-induced acetylene–vinylidene rearrangement have been investigated by computational methods.^{7–11} Calculations of reaction pathways for low-valent metals generally suggest that the M(HCCH)/M(CCH₂) rearrangement proceeds via a direct 1,2-shift mechanism.¹⁰ Whether the transferring species in this one-step mechanism is a proton (H⁺), hydrogen (H•), or hydride (H[−]) depends on the nature of the metal center. The metal acts to stabilize the lone pair electrons of the forming CCH₂ molecule while transferring an unpaired electron into an empty 2p orbital of the carbenic carbon. An alternative, two-step mechanism has been proposed in which the metal center plays a more active role.¹² The metal first inserts into a C–H bond of the acetylene reactant, forming an alkynyl-(hydrido)metal intermediate, HMCCH. This intermediate then undergoes rearrangement via a 1,3-proton shift, yielding the M(CCH₂) product.^{7–9,11} The two-step mechanism is likely only important for reactions with high-valent transition metal atoms.

We examine here the 1,2-shift mechanisms of acetylene interacting with Na (s¹), Al (p¹), and Y (d¹) metal atoms. Our interest in the interactions of acetylene with these particular metals stems from previous theoretical and experimental work. Kasai has reported matrix-isolation ESR investigations of the Na-induced rearrangement.^{13,14} He found that photoirradiation of Na and acetylene, co-condensed in argon matrices, yielded

the Na(CCH₂) complex. Numerous theoretical studies^{6,15–19} of the Al(HCCH) and Al(CCH₂) complexes have been reported, including the reaction pathway for rearrangement.^{10,20,21} These studies were largely prompted by matrix-isolation studies,^{22,23} suggesting that a vinyl radical-like Al–CH=CH structure is more stable than the anticipated Al(HCCH) π complex. Recent studies of Y + HCCH reactions led our interest in HCCH rearrangements on Y. Davis and co-workers²⁴ have studied collisions of Y atoms with acetylene using the crossed molecular beam method, focusing on collision energies that yield the H atom and H₂ elimination products. Siegbahn²⁵ has investigated the insertion of Y into acetylene to form an alkynyl(hydrido) complex, HYCCH.

A central focus of the present study is developing a qualitative picture of the electronic aspects of acetylene–vinylidene rearrangement. We are particularly interested in understanding how the bonds and lone pairs (the Lewis representation) of the acetylene reactant are transformed into the bonds and lone pairs of the vinylidene product. The application of the natural bond orbital (NBO) methods for determining the orbital interactions that promote acetylene isomerization and electron redistribution is demonstrated. NBO analysis readily identifies the leading Lewis representations of the reactant and product states. We show how similar analysis of the transition states can be used to determine the redistribution of electrons along reaction pathways.

Methods

All geometry optimizations were performed at the B3LYP level.²⁶ Dunning's augmented correlation-consistent double- ζ basis sets²⁷ were employed for the first- and second-row elements (aug-cc-pVDZ for H, C, and Al; cc-pVDZ for Na). The Stuttgart 28-electron quasi-relativistic effective core potential²⁸ and Peterson's cc-pRVDZ (7s7p5d1f)/[4s4p3d1f] valence basis set²⁹ were used for Y. Calculations at this level are referred to as B3LYP/aVDZ. The identities (equilibrium, transition state) of all optimized geometries were determined by frequency calculations, and zero-point energy (ZPE) cor-

* Corresponding author. E-mail: ericg@carbon.indstate.edu.

reactions were applied to all energies. Intrinsic reaction coordinate (IRC) calculations of the transition states were performed to identify reaction pathways. The B3LYP geometry optimization, frequency, and IRC calculations were performed with Gaussian 98.³⁰ The optimizations used Gaussian's "tight" convergence threshold to ensure adequate convergence of the geometrical features.

Single-point energy evaluations of the B3LYP/aVDZ geometries were performed using the restricted coupled-cluster method, RCCSD(T), with double-, triple-, and quadruple- ζ basis sets (aug-cc-pVXZ for H, C, and Al; cc-pVXZ for Na; cc-pRVXZ for Y²⁹). The triple- and quadruple- ζ basis sets for Y are respectively [6s6p4d2f1g] and [7s7p5d3f2g1h] contractions of (10s10p7d2f1g) and (12s12p9d3f2g1h) primitive sets. Calculations of the HCCH and CCH₂ radical anions required extra diffuse functions to describe the delocalized electron distribution. Dunning's doubly augmented d-aug-cc-pVXZ sets were used for these cases. RCCSD(T) energies at the complete basis set limit, $E(\text{CBS})$, were estimated by extrapolating the correlation-consistent energies, $E(X)$, using the mixed (exponential + Gaussian) fitting function³¹

$$E(X) = E(\text{CBS}) + Ae^{-(X-1)} + Be^{-(X-1)^2} \quad (1)$$

X in this equation represents the cardinal number of the basis set ($X = 2, 3, 4$ for DZ, TZ, QZ, respectively) and $E(\text{CBS})$, A , and B are fitting parameters. All valence electrons were correlated in the RCCSD(T) calculations. Correlation of high-energy core electrons (2s, 2p on Na and 4s, 4p on Y) was treated using triple- ζ basis sets with Peterson's core-correlating functions (cc-pwCVTZ for Na and tight s, p, d, f shells for Y).²⁹ Core-correlation corrections were applied to the RCCSD(T)/CBS energies for all structures involving Na and Y. Additional details of the basis set extrapolations and core-correlation corrections are provided in the Appendix. The RCCSD(T) calculations were performed with MOLPRO.³² Unless otherwise noted, all energies reported here are RCCSD(T)/CBS//B3LYP/aVDZ values with ZPE corrections.

The NBO method³³ was used to identify the best Lewis structure representations of the equilibrium geometries and to determine the transformation of the reactant Lewis structure into that of the product. We sought to determine this transformation by examining the nature of the transition state, which is generally poorly described by a single Lewis structure. Two separate NBO analyses were performed on the transition state. In the first analysis, we requested (using the directed \$CHOOSE search) that the NBO program identify the optimal set of bonding and nonbonding orbitals consistent with the reactant-like Lewis structure. These orbitals are optimal in the sense that they describe as much of the total electron density as possible. We denote this set of reactant-like NBOs $\{\sigma^R\}$. Similarly, we performed a second analysis, again on the transition state, now directing NBO to identify a set of bonding and nonbonding orbitals consistent with the product-like Lewis structure. This second set of NBOs is denoted $\{\sigma^P\}$. It is convenient to expand the natural localized molecular orbitals (NLMOs) of the transition state using the $\{\sigma^R\}$ and $\{\sigma^P\}$ NBO sets.

$$\psi_{\text{NLMO}} = \sum_i c_i \sigma_i^R = \sum_j d_j \sigma_j^P \quad (2)$$

By comparing these two expansions of a common set of NLMOs $\{\psi\}$, one can readily determine which NLMOs transform their character along the reaction pathway and, importantly, how the

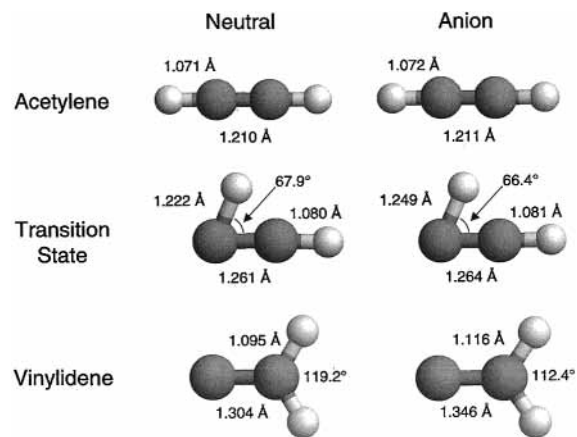


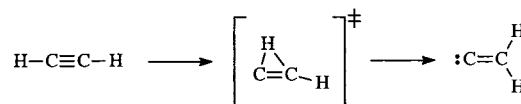
Figure 1. B3LYP/aVDZ optimized geometries of neutral and anion structures that characterize acetylene–vinylidene rearrangement. The transition state and CCH₂ structures exhibit C_s and C_{2v} symmetry, respectively.

bonding and nonbonding orbitals of the reactant correlate with those of the product.

In the following discussion, we refer to the orientations of some orbitals with respect to the Cartesian coordinate system. This coordinate system is defined such that the nuclei of a planar C_{2v} molecule lie in the yz plane with the C₂ axis aligned with the z -axis.

Results

Rearrangement of HCCH and Its Anion. We first consider the rearrangements of neutral HCCH and its anion in the absence of a metal atom.¹



Our interest in the anion system stems from the suggestion^{14,34} that metal atoms potentially facilitate acetylene–vinylidene rearrangement by prior electron transfer to form the charge-transfer complex $\text{M}^+(\text{HCCH}^-)$. We refer to the sp -hybridized atom of CCH₂ as C_α and the sp^2 -hybridized as C_β. Rearrangement, therefore, transfers hydrogen from C_α to C_β.

Optimized geometries of the equilibrium and transition state structures are shown in Figure 1. The transition state corresponds to a planar structure with a H atom in a bridging position and a C–C bond length (1.261 Å) that is somewhat elongated relative to that of HCCH (1.210 Å). The C–C bond further lengthens to 1.304 Å as the rearrangement proceeds to CCH₂, consistent with the nominal reduction in bond order from three to two. In CCH₂, the sp hybridization of C_α and the hyperconjugative interactions of the C_β–H bonds with the formally unoccupied 2p_y orbital of C_α yield an equilibrium C–C bond length that is somewhat shorter than a standard double bond length (1.335 Å in ethylene).

Ionization has only marginal influence on the geometries of HCCH and the transition state. The similarity of the neutral and anion geometries results from the diffuse nature of the unpaired electron of the anion. NBO analysis reveals that the unpaired electron resides entirely in Rydberg orbitals of HCCH and that 80% of its density remains in these orbitals in the transition state. The HCCH anion and transition state geometries are best described as those of the neutral systems, weakly perturbed by a diffuse electron.

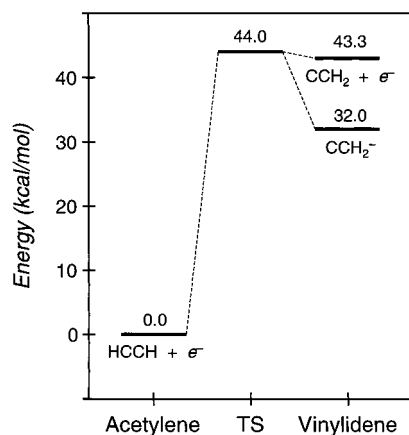


Figure 2. Potential energy diagram for acetylene–vinylidene rearrangement.

The ionization of CCH_2 leads in an anion geometry that differs rather significantly from that of neutral CCH_2 . Most notably, the C–C bond lengths of the anion (1.346 Å) and neutral (1.304 Å) differ by more than 0.04 Å. The C_α center of neutral CCH_2 is electron deficient with a formally vacant $2p_y$ orbital. Hyperconjugative interactions of this orbital with the C_β –H bonds shorten the C–C bond to 1.304 Å. The unpaired electron of CCH_2 anion predominantly occupies the C_α $2p_y$, significantly diminishing the strengths of the hyperconjugative interactions and thereby lengthening the C–C bond to 1.346 Å.²

Figure 2 shows the potential energy diagram for the neutral and anionic rearrangements. The neutral rearrangement is strongly endothermic, by 43.3 kcal/mol, proceeding via a barrier of 44.0 kcal/mol. Clearly, CCH_2 is highly unstable. A barrier of only 0.7 kcal/mol must be overcome for CCH_2 to revert to HCCH. The features of our reaction surface are in reasonable agreement with the best estimates for the endothermicity (42.95 kcal/mol at 0 K) and barrier (44.5 kcal/mol) from an extended basis set study recently reported by Yu and co-workers.³

The unpaired electron in the anionic rearrangement has no significant influence on the potential energy surface until CCH_2 is essentially fully formed. The HCCH anion and its transition state are, in fact, unstable with respect to electron release.^{1,2} For example, at the CCSD(T)/d-aug-cc-pVQZ level, we calculate negative electron affinities of -0.168 and -0.055 eV, respectively. In contrast, CCH_2 has a positive electron affinity of 0.492 eV [CCSD(T)/CBS], in reasonable agreement with the experimental value³⁵ of 0.47 ± 0.02 eV. Anionic rearrangement thus proceeds from neutral HCCH through the neutral transition state. The unpaired electron remains delocalized along this portion of the reaction pathway and then localizes in the C_α $2p_y$ orbital as CCH_2 forms. Whereas the unpaired electron has essentially no influence on the stability of HCCH and the transition state, it stabilizes CCH_2 by 11.3 kcal/mol. The endothermicity of the anionic rearrangement is 32.0 kcal/mol. Note that this value is determined with respect to $\text{HCCH} + e^-$ rather than the unstable HCCH^- . Frenking¹ and Sakai and Morokuma¹⁰ examined the HCCH anion rearrangement using 6-31G** and 6-311G** basis sets. In contrast to the results of Figure 2, they found the anion reaction to be nearly thermo-neutral, an artifact of the use of restricted basis sets.

We now consider the mechanism by which the bonds of HCCH undergo rearrangement to give the bonds and lone pair of CCH_2 . Table 1 compares the HCCH- and CCH_2 -like NBO analyses of the transition state. Of the seven occupied molecular orbitals, five (NLMOs 1, 2, 5–7) are identical in the two

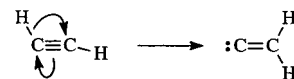
TABLE 1: NBO Analysis of the Acetylene–Vinylidene Transition State^a

NLMO	HCCH-like (R)			CCH ₂ -like (P)		
	%	(c)	σ^R	%	(d)	σ^P
1	95.3	(0.976)	$\sigma(\text{C}_\alpha\text{--C}_\beta)$	93.2	(0.966)	$\sigma(\text{C}_\alpha\text{--C}_\beta)$
2	99.9	(1.000)	$\pi(\text{C}_\alpha\text{--C}_\beta)$	99.9	(1.000)	$\pi(\text{C}_\alpha\text{--C}_\beta)$
3	92.0	(0.959)	$\pi(\text{C}_\alpha\text{--C}_\beta)$	40.9	(0.640)	$n(\text{C}_\alpha)$
	6.4	(0.253)	$\sigma^*(\text{C}_\alpha\text{--H})$	30.8	(0.555)	$\sigma(\text{C}_\beta\text{--H})$
4	84.7	(0.920)	$\sigma(\text{C}_\alpha\text{--H})$	15.9	(-0.399)	$2p(\text{C}_\alpha)$
	8.0	(0.283)	$\pi^*(\text{C}_\alpha\text{--C}_\beta)$	37.5	(0.612)	$n(\text{C}_\alpha)$
				29.3	(-0.542)	$\sigma(\text{C}_\beta\text{--H})$
5	98.6	(0.993)	$\sigma(\text{C}_\beta\text{--H})$	16.6	(0.408)	$2p(\text{C}_\alpha)$
6	100.0	(1.000)	$1s(\text{C}_\alpha)$	98.7	(0.993)	$\sigma(\text{C}_\beta\text{--H})$
7	100.0	(1.000)	$1s(\text{C}_\beta)$	100.0	(1.000)	$1s(\text{C}_\alpha)$
				99.9	(1.000)	$1s(\text{C}_\beta)$

^a B3LYP/aVDZ values. Leading contributions are listed for the HCCH-like and CCH_2 -like NBO expansions of the NLMOs. Percentage contributions are the squares of the corresponding expansion coefficients (cf. eq 2).

analyses. NLMO 1, for example, is the C–C σ bond in both HCCH and CCH_2 Lewis structures. It is reasonable to assume that these five orbitals remain essentially inactive (except for rehybridization) during the reaction. Only NLMOs 3 and 4 differ significantly in the two analyses. NLMO 3 is principally the in-plane π bond in the HCCH-like analysis but is a combination of a nonbonding hybrid (n) on C_α and the newly forming C_β –H bond in the CCH_2 -like analysis. NLMO 4 is the dissociating C_α –H bond of HCCH but is a mixture of the C_α nonbonding and C_β –H bond orbitals of CCH_2 . NBO analysis thus suggests that the chemically active orbitals in the acetylene–vinylidene rearrangement are the C_α –H and in-plane π orbitals of HCCH that respectively undergo transformation into the C_β –H and nonbonding C_α orbitals of CCH_2 .

Closer examination of the HCCH-like NBOs of the transition state suggests a simple qualitative description of these orbital transformations. We find that the in-plane π -type NBO is nearly 60% polarized toward C_α (50% = unpolarized). This orbital increasingly polarizes toward C_α as the system proceeds along the reaction path from the transition state to CCH_2 , eventually becoming the C_α lone pair of CCH_2 . Polarization of the π bond toward C_α leads to reverse polarization of its corresponding π^* toward C_β . As the H atom shifts around C_α into a bridging position, its bond to C_α begins to interact with the π^* orbital, increasingly centered on C_β . This $\sigma \rightarrow \pi^*$ interaction simultaneously promotes the cleavage of the C_α –H bond (by depleting electron density from σ), the cleavage of the C–C π bond (by populating π^*), and the formation of the C_β –H bond (by strengthening the overlap of the H $1s$ orbital with a C_β hybrid). In short, the rearrangement of electrons for the acetylene–vinylidene reaction can be represented using the following curved-arrow diagram. Full-headed arrows are used to indi-



cate the movement of electron pairs. The in-plane π bond of HCCH increasingly polarizes toward C_α to become the CCH_2 lone pair. Hydride (H^-) simultaneously shifts from C_α to C_β . Sakai and Morokuma¹⁰ similarly concluded, based on a charge-centroid analysis of Foster–Boys localized orbitals, that acetylene–vinylidene rearrangement proceeds via a 1,2-hydride shift.

HCCH anion rearrangement also proceeds via a 1,2-hydride shift with the unpaired electron remaining delocalized until late in the reaction when it enters the C_α $2p_y$ orbital of CCH_2 . The

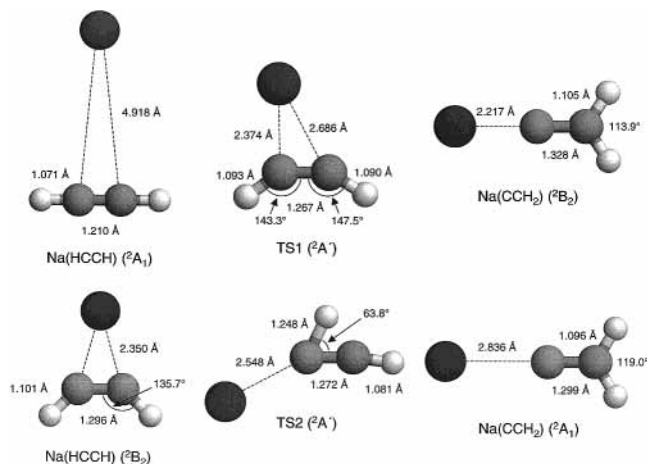


Figure 3. B3LYP/aVDZ optimized geometries of the equilibrium and transition state structures for Na-induced acetylene–vinylidene rearrangement.

TABLE 2: Energies and Lewis Representations of the Equilibrium Structures for Na-Induced Acetylene–Vinylidene Rearrangement

structure	state	energy ^a	Lewis representation ^b
Na + HCCH	$^2S + ^1\Sigma_g^+$	0.0	$\overset{\cdot}{\text{Na}}$
Na(HCCH)	2A_1	-0.3	$\text{H}-\text{C}\equiv\text{C}-\text{H}$
Na(HCCH)	2B_2	11.2	$\begin{array}{c} \text{Na} \qquad \text{Na} \\ \text{H}-\overset{\cdot}{\text{C}}=\overset{\cdot}{\text{C}}-\text{H} \quad \text{H}-\text{C}\equiv\text{C}-\text{H} \end{array}$
Na(CCH ₂)	2B_2	10.5	$\text{Na} \quad \text{:}\overset{\cdot}{\text{C}}=\overset{\cdot}{\text{C}}\text{H}$
Na(CCH ₂)	2A_1	41.4	$\text{Na}\cdot \quad \text{:}\overset{\cdot}{\text{C}}=\overset{\cdot}{\text{C}}\text{H}$
Na + CCH ₂	$^2S + ^1A_1$	43.3	

^a RCCSD(T)/CBS//B3LYP/aVDZ values with ZPE and core-correlation corrections, in kcal/mol. ^b Two Lewis representations are given for structures having different bonding patterns in the α and β systems. In these cases, the first representation reflects the distribution of α electrons and the second that of the β electrons. See ref 37.

charge-centroid analysis of Sakai and Morokuma¹⁰ suggested a 1,2-hydrogen (H•) shift mechanism for anionic rearrangement. However, the hydrogen shift mechanism is an artifact of the restricted basis sets used in their study that effectively localize the unpaired electron on the hydrocarbon throughout the reaction. Jensen et al.³⁶ have studied the collisionless decay rate of vinylidene anion ($\text{CCH}_2^- \rightarrow \text{HCCH} + e^-$), noting that it is unclear when the electron is ejected during the isomerization. Our calculations suggest that the electron is lost early in this reaction, prior to the transition state.

Na-Induced Rearrangement. Previous theoretical studies of Na–acetylene and Na–vinylidene interactions have identified ground state geometries for 2A_1 Na(HCCH) and 2B_2 Na(CCH₂). Figure 3 shows the optimized equilibrium and transition state geometries for the Na(HCCH)/Na(CCH₂) system. Table 2 lists the energies of the equilibrium structures together with their Lewis representations. Figure 4 shows the potential energy diagram for Na-induced rearrangement.

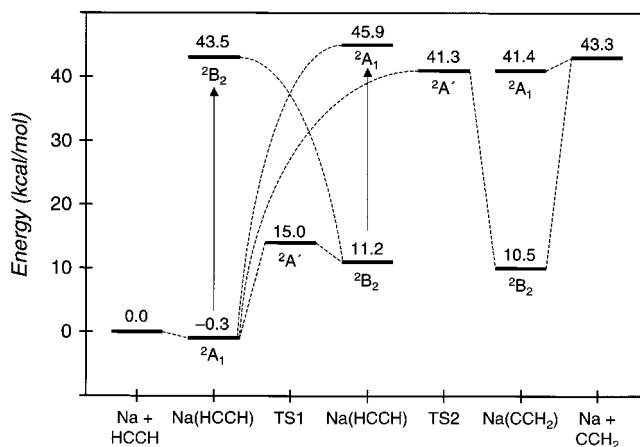
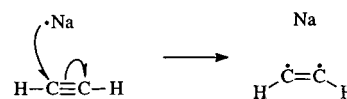


Figure 4. RCCSD(T)/CBS potential energy diagram for Na-induced acetylene–vinylidene rearrangement. The arrows represent vertical excitation of the ground state (at its equilibrium geometry) into the lowest excited state of the specified symmetry.

Two ground state equilibrium geometries were examined for Na(HCCH), both exhibiting π -type structures of C_{2v} symmetry. The lower energy structure is the 2A_1 van der Waals complex, bound by only 0.3 kcal/mol. Its geometry resembles that of free HCCH, weakly perturbed by the distant 2S Na atom. The higher energy structure, lying 11.1 kcal/mol above the reactants, is the 2B_2 charge-transfer complex, $\text{Na}^+(\text{HCCH}^-)$, in which the unpaired electron has transferred to the in-plane HCCH π^* . The vertical excitation energy to the 2A_1 configuration ($\pi^* \rightarrow 3s$) at the 2B_2 optimized geometry is 34.7 kcal/mol. NBO analysis of the 2B_2 complex yields a pair of Lewis structures³⁷ (cf. Table 2) that reflect the differing bonding characteristics of the α and β electrons.

The 2B_2 charge-transfer complex can be obtained in two ways from the 2A_1 van der Waals complex. First, $\text{Na } 3s \rightarrow 3p_y$ promotion of the 2A_1 complex (vertical excitation energy = 43.8 kcal/mol) yields the 2B_2 configuration. Geometry relaxation leads to the equilibrium charge-transfer structure as the unpaired electron transfers into the HCCH π^* . Second, the 2A_1 complex can follow a C_s pathway, through the transition state TS1, to the 2B_2 complex. TS1 lies 15.0 kcal/mol above the reactants, or 15.3 kcal/mol above the van der Waals complex. Moving the Na atom, in TS1, off the C_2 symmetry axis allows the Na 3s electron to transfer into the in-plane π^* of HCCH, cleaving the π bond in the α system and leaving a nonbonding α electron on both C centers. This rearrangement of electrons can be represented by the following α -spin Lewis structures.³⁷ Note



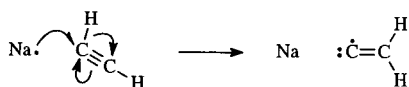
that the lines and dots of these structures reflect the bonding and nonbonding character of the α electrons only. Fishhook arrows are used, as usual, to show movement of single electrons. The β systems of 2A_1 and 2B_2 Na(HCCH) are described by a common Lewis structure (cf. Table 2), suggesting that the β electrons do not undergo rearrangement along the TS1 pathway.

The Na(CCH₂) complex has a 2B_2 ground state configuration with the unpaired electron predominantly localized in the in-plane $2p_y$ orbital on C_α . The equilibrium geometry corresponds to that of a charge-transfer complex, $\text{Na}^+(\text{CCH}_2^-)$, and is 10.5 kcal/mol less stable than the reactants. We note that the endothermicity of the Na-induced rearrangement (10.8 kcal/mol)

is substantially less than that (32.0 kcal/mol) of the HCCH + e⁻/CCH₂⁻ rearrangement. In both cases, the unpaired electron localizes on CCH₂, stabilizing the electron-deficient C_α center relative to that of neutral CCH₂. The Na(CCH₂) complex is further stabilized by the electrostatic interaction of the Na⁺ and CCH₂⁻ fragments. An excited ²A₁ Na(CCH₂) complex results from the interaction of ²S Na with ¹A₁ CCH₂. At its equilibrium geometry, the ²A₁ complex lies 30.9 kcal/mol above the ²B₂ Na(CCH₂) complex. It is unlikely that this excited state complex plays any significant role in the acetylene–vinylidene rearrangement.

A transition state, TS2, was identified for the Na-induced rearrangement. An IRC calculation reveals that TS2 lies along a C_s reaction pathway connecting the ²A₁ Na(HCCH) and ²B₂ Na(CCH₂) complexes. The transition state is 41.3 kcal/mol less stable than the reactants, but is slightly more stable (by 2.7 kcal/mol) than the transition state for the metal-free reaction (cf. Figure 2). Donation of Na 3s electron density to the increasingly electron deficient C_α center of the forming CCH₂ molecule slightly stabilizes TS2 relative to that of the metal-free reaction. Attempts to identify a reaction pathway connecting ²B₂ Na(HCCH) to ²B₂ Na(CCH₂) failed. Sakai and Morokuma¹⁰ identified a ²B₂ → ²B₂ pathway for Li-induced rearrangement but were likewise unable to locate the corresponding pathway for the Na-induced reaction.

Na-induced rearrangement proceeds via hydride transfer. NBO analysis reveals the following mechanism. Again, the



fishhook arrow is used to indicate the movement of a single electron while full-headed arrows show the movements of electron pairs. The mechanism is similar to that of the metal-free reaction. As the system proceeds along the reaction pathway, the in-plane π bond increasingly polarizes toward C_α (eventually forming the lone pair of CCH₂) and hydride shifts from C_α to C_β. The Na center facilitates the 1,2-hydride shift by transferring its 3s electron into a valence hybrid on C_α. Sakai and Morokuma¹⁰ similarly concluded that Na-induced rearrangement proceeds via a hydride transfer mechanism.

Finally, the features of our calculated potential energy diagram (Figure 4) are largely consistent with those anticipated from Kasai's matrix-isolation studies.^{13,14} No rearrangement was observed from the interaction of ground state Na atoms with acetylene due to the large activation barrier (~41 kcal/mol in Figure 4) and the cryogenic conditions (~4 K) of the argon matrixes. However, exposing the matrixes to yellow light (λ = 600 ± 50 nm) for several minutes yielded Na(CCH₂). Kasai proposed a mechanism for rearrangement based on the absorption of two photons.¹⁴ The first photon promotes Na to its ²P excited state, which subsequently forms a Na⁺(HCCH⁻) charge-transfer complex. The photon energy (600 nm = 48 kcal/mol) is clearly consistent with the vertical excitation energy (43.8 kcal/mol) of the van der Waals complex. It was proposed that a second photon then excites the π_x → π_z^{*} (out-of-plane to in-plane) transition of the charge-transfer complex, which subsequently undergoes rearrangement to Na(CCH₂). Absorption of a second photon would clearly provide sufficient energy for the system to surmount the 41 kcal/mol barrier. However, our calculations suggest that π_x → π_z^{*} excitation is unlikely. This excitation gives rise to a ²B₁ configuration that lies about 68 kcal/mol above the ²B₂ charge-transfer state, well above the energy of a yellow photon.

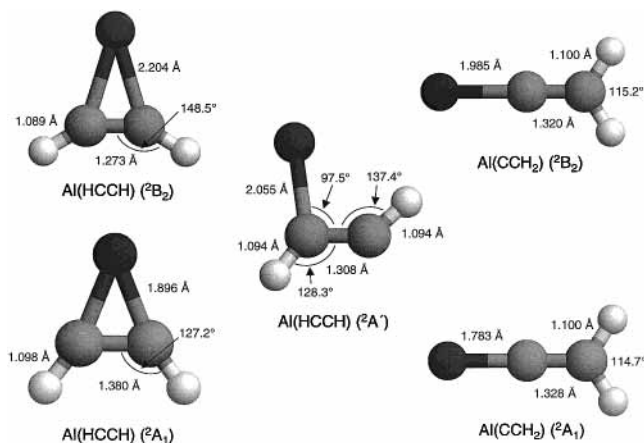
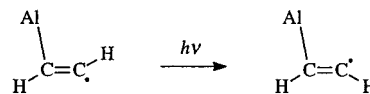


Figure 5. B3LYP/aVDZ optimized geometries of the equilibrium structures for Al-induced acetylene–vinylidene rearrangement.

Al-Induced Rearrangement. Numerous theoretical studies of Al(HCCH) and Al(CCH₂) have been reported.^{6,10,15–21} Many of these were prompted by Kasai's matrix-isolation studies^{22,23} of Al(HCCH) suggesting a vinyl-like σ-bonded equilibrium structure with a trans arrangement of the H atoms. Irradiation of the matrixes with visible light led to changes in the ESR spectra consistent with trans → cis isomerization. No π-type complex was observed.

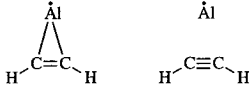
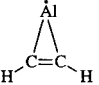
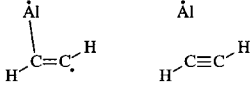
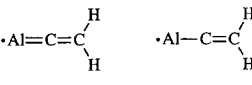
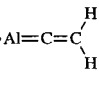


Theoretical studies have generally identified three stable forms of Al(HCCH): a ²B₂ π complex, a ²A₁ π complex, and the ²A' trans σ complex. The ²A' cis σ complex is only stable at uncorrelated levels of theory, reverting to the ²B₂ form when optimized with correlated methods.^{16,17} High-level calculations generally suggest that ²B₂ Al(HCCH) is the most stable structure. The only equilibrium structure previously reported for Al(CCH₂) is that of the ²B₂ state.

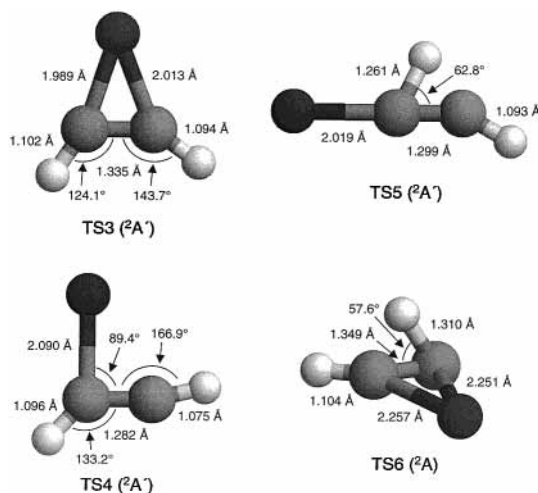
Figure 5 shows the B3LYP/aVDZ optimized structures for Al(HCCH) and Al(CCH₂). Table 3 gives the energies and Lewis representations for these structures. The ²B₂ Al(HCCH) complex is bound by 20.5 kcal/mol with respect to the separated Al and HCCH reactants. NBO analysis reveals partial metallacyclopene character (only in the α system) with the Al nonbonding electrons occupying the 3s orbital. The Al–C bonds of the α-spin Lewis structure arise from the overlap of Al 3p hybrids (3p_z ± 3p_y) with hybrids of high p character (86%) on the C centers. These bonds are strongly polarized (87%) toward C. The ²A₁ state (at –20.3 kcal/mol) is only marginally less stable than the ²B₂ state. NBO analysis reveals full metallacyclopene character (Al–C bonds in both the α and β systems) of ²A₁ Al(HCCH), consistent with its shorter Al–C bonds, longer C–C bond, and more strongly bent H–C–C angles. The trans σ-bonded complex is bound by 16.4 kcal/mol. Attempts to identify the cis isomer failed, with all optimizations reverting to the ²B₂ π complex.

The ²B₂ and ²A₁ states of Al(CCH₂) were optimized. The ²B₂ Al(CCH₂) complex (at –23.3 kcal/mol) was the most stable of all AlC₂H₂ isomers examined in this work. It exhibits partial metallallene character with the unpaired electron residing in a b₂ Al–C π bond. Strongly polarized (90%) toward C_α, the π bond arises from the overlap of the Al 3p_y with the C_α 2p_y. The overlap of the Al 3p_z with a C_α sp hybrid gives rise to a similarly polarized Al–C σ bond. The ²A₁ Al(CCH₂) complex exhibits

TABLE 3: Energies and Lewis Representations of the Equilibrium Structures for Al-Induced Acetylene–Vinylidene Rearrangement

structure	state	energy ^a	Lewis representation ^b
Al + HCCH	$^2P + ^1\Sigma_g^+$	0.0	
Al(HCCH)	2B_2	-20.5	
Al(HCCH)	2A_1	-20.3	
Al(HCCH)	$^2A'$	-16.4	
Al(CCH2)	2B_2	-23.3	
Al(CCH2)	2A_1	6.8	
Al + CCH2	$^2P + ^1A_1$	43.3	

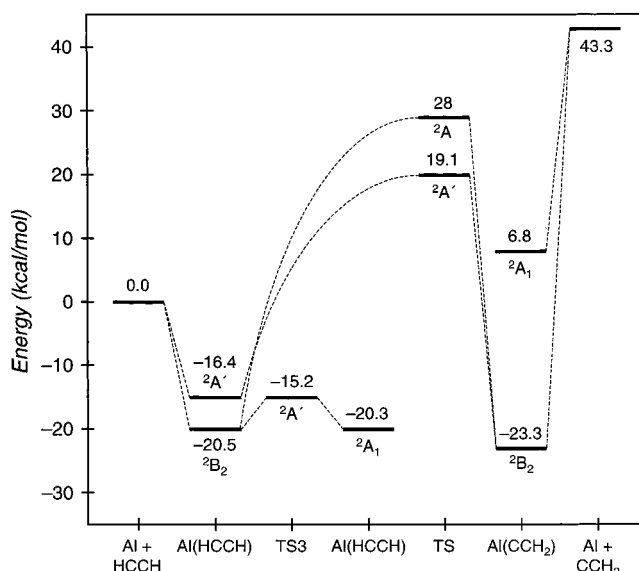
^a RCCSD(T)/CBS//B3LYP/aVDZ values with ZPE corrections, in kcal/mol. ^b Two Lewis representations are given for structures having different bonding patterns in the α and β systems. In these cases, the first representation reflects the distribution of α electrons and the second that of the β electrons. See ref 37.

**Figure 6.** B3LYP/aVDZ optimized transition state structures for Al-induced acetylene–vinylidene rearrangement.

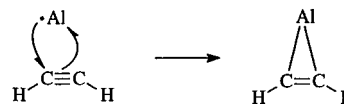
full metallaallene character and, hence, a shorter Al–C bond. The 2A_1 state is considerably less stable (by 30.1 kcal/mol) than the 2B_2 state and will not be considered further.

Four transition states were identified for the Al(HCCH)/Al(CCH₂) system. Figure 6 shows the optimized structures, and Figure 7 shows the resulting potential energy diagram. Two of the transition states, TS3 and TS4, reside along pathways that connect the three equilibrium Al(HCCH) structures. The small barriers associated with these transition states suggest that the three equilibrium Al(HCCH) structures will readily interconvert at moderate temperatures.

TS3 is a C_s structure of $^2A'$ configuration along a pathway connecting the 2B_2 and 2A_1 π complexes. Whereas it has been suggested¹⁷ that a high activation barrier precludes the formation of the 2A_1 complex from the 2B_2 under normal conditions, we

**Figure 7.** RCCSD(T)/CBS potential energy diagram for Al-induced acetylene–vinylidene rearrangement.

find that the C_s pathway through TS3 has a barrier of only 5.3 kcal/mol. This pathway is associated with the following redistribution of electrons in the β system.



As the Al center shifts off the symmetry axis, its 3s electron delocalizes into the HCCH π^* , forming an Al–C bond. The π electron simultaneously undergoes back-donation into an empty Al hybrid, thereby forming a second Al–C bond. The resulting bond length changes are consistent with the bond order changes reflected by these Lewis structures. No redistribution of electrons is necessary in the α system since the 2B_2 and 2A_1 states are represented by the same metallacyclopropene Lewis structure.

TS4 lies on a C_s pathway that interconverts the 2B_2 and 2A_1 complexes. Comparison of the Lewis representations (cf. Table 3) for these states reveals that the TS4 pathway simply cleaves an α Al–C bond. The barrier for $^2B_2 \rightarrow ^2A_1$ conversion is 4.0 kcal/mol. We note that the $^2A' \rightarrow ^2B_2$ barrier is 0.7 kcal/mol at the B3LYP/aVDZ level but decreases to 0.1 and 0.0 kcal/mol for RCCSD(T)/aVTZ and RCCSD(T)/aVQZ, respectively. The diminishing barrier suggests that the $^2A'$ complex is unstable and will potentially revert to the 2B_2 form if optimized at the highest levels of theory.

Two additional transition states reside along pathways that characterize Al(HCCH)/Al(CCH₂) rearrangement. TS5, the lower energy structure at 19.1 kcal/mol above the reactants, lies along a C_s pathway that connects $^2A'$ Al(HCCH) to 2B_2 Al(CCH₂). A similar transition state, although of C_1 symmetry, was previously reported by Flores and Largo.²¹ TS6, the higher energy structure at ca. 28 kcal/mol, lies along a C_1 pathway that connects 2B_2 Al(HCCH) to 2B_2 Al(CCH₂). Attempts to locate a reaction pathway involving 2A_1 Al(HCCH) failed. We will focus our attention on the reaction mechanism for the TS5 pathway, likely the predominant pathway for Al-induced rearrangement. Note that the 19.1 kcal/mol barrier along the TS5 pathway is of considerably lower energy than the 41.3 kcal/mol barrier for Na-induced rearrangement. Covalent Al–C interactions stabilize the Al-induced pathway relative to that of Na.

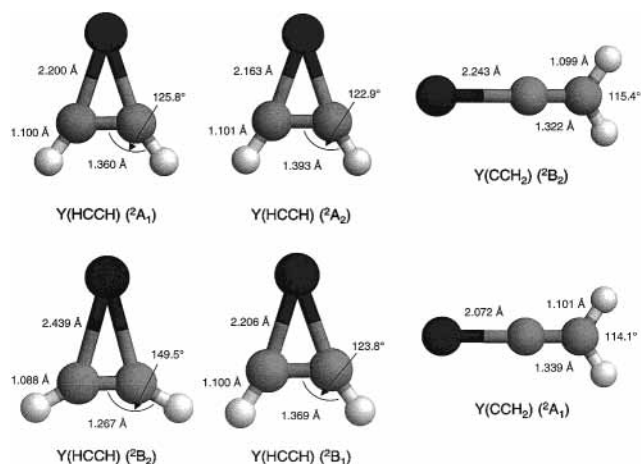


Figure 8. B3LYP/aVDZ optimized geometries of the equilibrium structures for Y-induced acetylene–vinylidene rearrangement.

The reactant- and product-like NBO analyses of TS5 reveal differing rearrangements of α and β electrons. We are compelled, therefore, to write different mechanisms for different spins. The result is the following representation in which four valence electrons (two α and two β) undergo simultaneous rearrangement. Four fishhook arrows are used to show movements of these electrons.

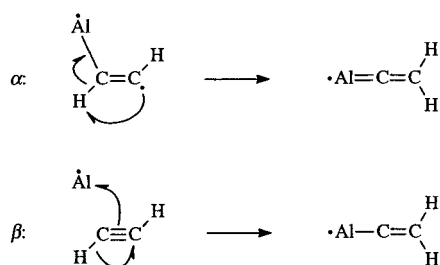


Figure 9. B3LYP/aVDZ optimized transition state structures for Y-induced acetylene–vinylidene rearrangement.

TABLE 4: Energies and Lewis Representations of the Equilibrium Structures for Y-Induced Acetylene–Vinylidene Rearrangement

structure	state	energy ^a	Lewis representation ^b
Y + HCCH	² D + ¹ Σ_g^+	0.0	
Y(HCCH)	² A ₁	-47.7	
Y(HCCH)	² B ₂	-26.6	
Y(HCCH)	² A ₂	-19.9	
Y(HCCH)	² B ₁	-14.2	
Y(CCH ₂)	² B ₂	-24.5	
Y(CCH ₂)	² A ₁	-22.2	
Y + CCH ₂	² D + ¹ A ₁	43.3	

^a RCCSD(T)/CBS//B3LYP/aVDZ values with ZPE and core-correlation corrections, in kcal/mol. ^b Two Lewis representations are given for structures having different bonding patterns in the α and β systems. In these cases, the first representation reflects the distribution of α electrons and the second that of the β electrons. See ref 37.

Y-Induced Rearrangement. Figures 8 and 9 show the optimized equilibrium and transition state geometries for the Y(HCCH)/Y(CCH₂) system. Table 4 lists the energies and Lewis representations of the various equilibrium structures. Figure 10 shows the potential energy diagram for the Y-induced rearrangement.

We optimized π complexes for Y(HCCH) corresponding to the lowest energy states of the four irreducible representations of C_{2v} symmetry. The most stable of these is ²A₁ Y(HCCH), bound by 47.7 kcal/mol with respect to the separated reactants. The Lewis representation of this state is that of a metallacyclopene with the unpaired electron residing in the Y 5s orbital. The Y–C bonds are formed from the overlap of a Y d-type hybrid ($4d_{yz} \pm 4d_{z^2}$) with C hybrids of $sp^{2.7}$ character.

Consider the rearrangement of electrons in the α system. As the H nucleus moves around C _{α} toward C _{β} , the C _{α} –H bond begins to interact with the nonbonding electron on C _{β} (through an $n_C \rightarrow \sigma_{CH}^*$ interaction). This interaction cleaves the C _{α} –H bond, by populating its antibond, as the new C _{β} –H bond forms from the overlap of n_C with the H 1s. As H departs, the α electron remaining on C _{α} increasingly delocalizes into an Al 3p orbital, resulting in the formation of a polarized Al–C π bond.

The β system reveals a different rearrangement of electrons. The in-plane π bond polarizes toward C _{α} (it is already 90% polarized toward C _{α} in TS5) and delocalizes into a vacant Al 3p orbital. The π bond thereby breaks and a new Al–C bond forms. (Note that C _{α} undergoes rehybridization during the reaction so that the resulting Al–C bond is of σ -type.) As the π bond polarizes toward C _{α} , the π^* antibond polarizes toward C _{β} (90% C _{β} 2p in TS5). With H moving into a bridging position, the β electron of the C _{α} –H bond increasingly delocalizes into the π^* , through a $\sigma_{CH} \rightarrow 2p$ interaction. The interaction eventually cleaves the C _{α} –H bond and H shifts with the β electron to form the new C _{β} –H bond, thereby completing the valence at C _{β} .

The rearrangements of the α and β electrons together describe a 1,2-hydrogen shift mechanism, with an H nucleus and a β electron transferring from C _{α} to C _{β} . Sakai and Morokuma¹⁰ similarly concluded that Al-induced rearrangement proceeds via a hydrogen-transfer mechanism

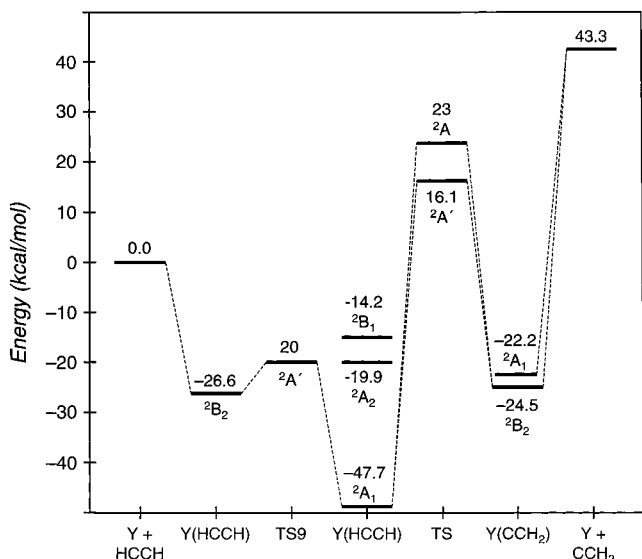


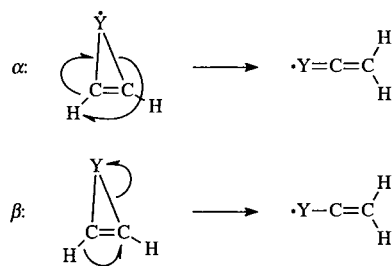
Figure 10. RCCSD(T)/CBS potential energy diagram for Y-induced acetylene–vinylidene rearrangement.

These bonds are strongly polarized (84%) toward the C centers. The excited 2A_2 and 2B_1 states (at -19.9 and -14.2 kcal/mol) have metallacyclopene Lewis representations and geometrical features similar to the 2A_1 ground state. The unpaired electrons in these states reside in the Y $4d_{xy}$ (2A_2) and $4d_{xz}$ (2B_1) orbitals. The 2B_2 state (at -26.6 kcal/mol) has only partial metallacyclopene character (in the α system). The unpaired electron occupies a b_2 orbital, which together with the a_1 π -type orbital of HCCH give rise to a pair of α -spin Y–C bonds. The nonbonding electrons on Y reside in the 5s orbital. The partial metallacyclopene character of the 2B_2 state yields geometrical features (long Y–C bond, short C–C bonds, large H–C–C angles) that differ significantly from those of the other three states.

The 2B_2 and 2A_1 states of Y(CCH₂) were optimized. 2B_2 Y(CCH₂) is the ground state (at -24.5 kcal/mol). It exhibits partial metallallene character similar to that of 2B_2 Al(CCH₂). The unpaired electron resides in a b_2 Y–C π bond formed from the overlap of the Y $4d_{yz}$ with the C $2p_y$ and strongly polarized (87%) toward C. The Y–C σ bond results from the overlap of a C sp hybrid with the Y $4d_{z^2}$ orbital, again strongly polarized (90%) toward C. In contrast to the Na and Al cases, the excited 2A_1 state (at -22.2 kcal/mol) is only slightly less stable than the ground state. The 2A_1 state exhibits full metallallene character with a short Y–C bond. The unpaired electron occupies the Y 5s.

We identified two transition states for Y-induced HCCH/CCH₂ rearrangement. TS7 and TS8 respectively lie on C_s and C_1 pathways that interconvert 2A_1 Y(HCCH) and 2B_2 Y(CCH₂). TS7, the lower energy transition state, lies 16.1 kcal/mol above the reactants, slightly lower than the 19.1 kcal/mol barrier for Al-induced rearrangement. TS8 lies approximately 7 kcal/mol above TS7. Attempts to identify reaction pathways involving the 2B_1 , 2B_2 , and 2A_2 states of Y(HCCH) or 2A_1 Y(CCH₂) failed.

The reaction along the TS7 pathway proceeds as follows. In the orientation shown below, the H and Y nuclei shift in a concerted counterclockwise fashion about C_α . Four electrons (two α and two β) undergo simultaneous rearrangement, similar to that revealed in the Al mechanism. In the α system, as Y moves away from C_β , the Y– C_β bonding electron shifts toward C_β and increasingly delocalizes in the C_α –H σ^* antibond. This shift in electron density cleaves the Y– C_β bond, cleaves the C_α –H bond, and forms the new C_β –H bond of CCH₂. As the



C_α –H bond cleaves, its electron begins to interact with a Y 4d hybrid, forming the Y– C_α π bond. Meanwhile, in the β system, the C_α –H bonding electron delocalizes into the Y– C_β σ^* antibond, cleaving both bonds and forming a new C_β –H bond. The electron of the Y– C_β bond shifts onto Y, becoming the 5s nonbonding electron of the product. Thus, Y-induced rearrangement involves a 1,2-hydrogen shift in which a H nucleus and a β electron transfer from C_α to C_β .

We attempted to identify the transition state along a C_s pathway connecting 2A_1 and 2B_2 Y(HCCH), analogous to TS3 of the Al system. Numerous optimizations of this state failed. However, all optimizations tended to converge toward a common structure lying ca. 7–8 kcal/mol above the 2B_2 state. This structure, TS9, is shown in Figure 9.

Conclusions

Metal-induced acetylene (HCCH)–vinylidene (CCH₂) rearrangement proceeds via simple 1,2-shifts in the gas phase. The metal centers stabilize the M(CCH₂) product by effectively transferring an electron to the carbenic center of the vinylidene fragment. The energies of the M(CCH₂) products are 43.3 (no metal, neutral), 32.0 (no metal, anion), 10.5 (Na), -23.3 (Al), and -24.5 (Y) kcal/mol relative to the separated M + HCCH reactants. The reaction barrier decreases from 44.0 kcal/mol in the metal-free rearrangement (neutral and anion) to 41.3 (Na), 19.1 (Al), and 16.1 (Y) kcal/mol in the metal-induced reactions.

Ground state Na (s^1) is not particularly effective at promoting HCCH–CCH₂ rearrangement. The barrier for the Na-induced reaction is only 2.7 kcal/mol less than that of the metal-free reaction. Na slightly stabilizes the transition state by transferring a small amount of its 3s electron density to the electron-deficient carbon of the forming CCH₂ molecule, but the transfer of a full electron does not occur until later in the rearrangement when CCH₂ is more fully formed. The resulting charge-transfer complex Na⁺(CCH₂[−]) is ca. 22 kcal/mol more stable than the free CCH₂[−] anion due to metal–ligand electrostatic interaction.

Al (p^1) and Y (d^1) facilitate the rearrangement to CCH₂. Both metals interact with HCCH to form strongly bound metallacyclopene structures. The covalent interactions of the metal centers with the hydrocarbon reduce the reaction barrier relative to the separated reactants, and the resulting M(CCH₂) products exhibit metallallene bonding patterns.

Natural bond orbital analysis of the HCCH–CCH₂ rearrangement has been used to determine the redistribution of electrons during the reaction. In the metal-free reactions (both neutral and anion), we find that rearrangement proceeds via a 1,2-hydride shift. The Na-induced reaction, which exhibits a similarly large barrier, likewise proceeds via a 1,2-hydride shift. The metal-free and Na-induced reactions involve heterolytic cleavage and formation of bonds in which electron pairs move together. In contrast, analysis of the Al- and Y-induced reactions reveals a 1,2-hydrogen shift mechanism. These reactions involve homolytic cleavage and formation of bonds in which the α and

β electron densities move in opposing directions. Homolytic bond cleavage and the redistribution of α and β density in opposing directions are general features of open-shell reaction mechanisms that involve different Lewis structures for different spins.

Acknowledgment. E.D.G. acknowledges Kirk Peterson (Washington State University) for advice regarding MOLPRO and basis set extrapolations. Prof. Peterson kindly provided his cc-pRVXZ basis sets for Y and the core-correlating functions for Na and Y prior to their publication. The Indiana State University College of Arts and Sciences and the Wabash Valley Section of the American Chemical Society provided research support for M.L.S. Partial support for this work was also provided by the National Science Foundation's Division of Undergraduate Education through Grant DUE 98-51497.

Appendix

We briefly describe here the extrapolations used to estimate complete basis set (CBS) limiting values for the RCCSD(T) energies. Table 5 provides details of these extrapolations (cf.

TABLE 5: Basis Set Extrapolations^{a,b}

structure	state	aVDZ	aVTZ	aVQZ	CBS ^c	core ^d	best estimate ^e
HCCH + e ⁻	¹ Σ_g^+	0.0	0.0	0.0	0.0		0.0
TS	¹ A'	40.9	43.4	43.8	44.0		44.0
CCH ₂ + e ⁻	¹ A ₁	37.6	42.3	43.0	43.3		43.3
CCH ₂ ⁻	² B ₂	27.0	31.3	31.8	32.0		32.0
Na(HCCH)	² A ₁	-0.2	-0.2	-0.3	-0.3	0.0	-0.3
TS1	² A'	14.4	14.8	14.5	14.4	0.6	15.0
Na(HCCH)	² B ₂	10.3	11.3	11.1	10.9	0.3	11.2
TS2	² A'	38.3	40.9	41.3	41.5	-0.2	41.3
Na(CCH ₂)	² B ₂	7.0	9.7	9.8	9.9	0.6	10.5
Na(CCH ₂)	² A ₁	36.1	40.5	41.2	41.4	0.0	41.4
Al(HCCH)	² B ₂	-16.7	-19.4	-20.1	-20.5		-20.5
Al(HCCH)	² A ₁	-12.6	-17.3	-19.2	-20.3		-20.3
Al(HCCH)	² A'	-14.6	-15.6	-16.1	-16.4		-16.4
TS3	² A'	-9.5	-13.1	-14.4	-15.2		-15.2
TS4	² A'	-13.4	-15.5	-16.1	-16.5		-16.5
TS5	² A'	20.9	19.7	19.3	19.1		19.1
TS6	² A	28.9	28.9	f			
Al(CCH ₂)	² B ₂	-22.4	-22.8	-23.1	-23.3		-23.3
Al(CCH ₂)	² A ₁	10.6	8.7	7.5	6.8		6.8
Y(HCCH)	² A ₁	-44.3	-44.5	-45.4	-45.9	-1.8	-47.7
		(-42.5)	(-44.1)	(-45.2)	(-45.9)		
Y(HCCH)	² B ₂	-25.6	-25.3	-25.6	-25.8	-0.8	-26.6
		(-24.0)	(-24.9)	(-25.5)	(-25.8)		
Y(HCCH)	² A ₂	-14.2	-14.5	-15.5	-16.1	-3.8	-19.9
		(-12.3)	(-14.0)	(-15.3)	(-16.1)		
Y(HCCH)	² B ₁	-11.9	-12.0	-12.7	-13.3	-0.9	-14.2
		(-10.1)	(-11.5)	(-12.5)	(-13.2)		
TS7	² A'	14.4	15.8	15.9	15.9	0.2	16.1
TS8	² A	21.3	22.9	f			
Y(CCH ₂)	² B ₂	-27.6	-25.2	-25.0	-25.0	0.5	-24.5
Y(CCH ₂)	² A ₁	-21.0	-20.5	-21.1	-21.5	-0.7	-22.2

^a All values are RCCSD(T) energies, in kcal/mol, relative to the energies of the separated M + HCCH reactants. The values in parentheses for Y(HCCH) are counterpoise (CP)-corrected. ^b The basis sets employed are the aug-cc-pVXZ sets for H, C, and Al, the cc-pVXZ sets for Na, and the cc-pRVXZ sets for Y (X = D, T, Q). The energies for CCH₂⁻ were evaluated with the doubly augmented d-aug-cc-VXZ sets. ^c Estimates of the CBS limit were generally obtained by extrapolating the raw RCCSD(T) energies using eq 1. The CBS limits for the CP-corrected energies were obtained by extrapolating the relative RCCSD(T) energies. ^d The core-correlation effect was evaluated as the difference of the energies of correlated-core (2s, 2p for Na and 4s, 4p for Y only) and frozen-core calculations. The core-valence basis sets cc-pwCVTZ (Na) and cc-pRCVTZ (Y) were used in these calculations. ^e The best estimate is the sum of the CBS and core-correlation energies. ^f Calculation exceeds the capabilities of our computational resources.

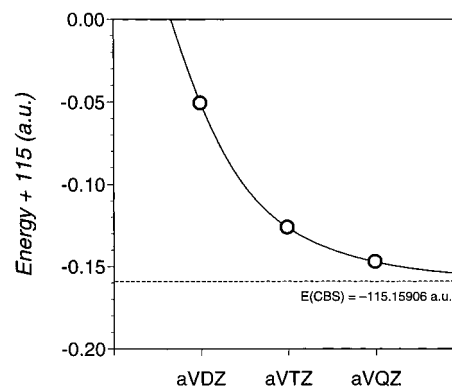


Figure 11. Extrapolation of the RCCSD(T) energy for ²A₁ Y(HCCH).

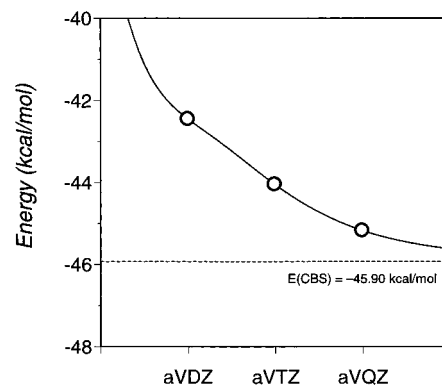


Figure 12. Extrapolation of the counterpoise-corrected RCCSD(T) energies for ²A₁ Y(HCCH).

eq 1). The “best estimate” values listed in the table are the energies reported elsewhere in this paper.

The relative energies of Table 5 often exhibit poor convergence with basis set extension. For example, for ²A₁ Y(HCCH), the aVDZ and aVTZ values (-44.3 and -44.5 kcal/mol, respectively) are essentially identical but differ by nearly 1 kcal/mol from the aVQZ value (-45.5 kcal/mol). In contrast, the raw energies, shown in Figure 11, reveal convergent behavior across the aVDZ–aVQZ series. Extrapolating the raw energy for ²A₁ Y(HCCH) provides an estimate for the CBS limit of -115.159 06 au. This value, together with the CBS limits for Y and HCCH (-37.863 41 and -77.221 12 au, respectively) and a ZPE correction of 0.9 kcal/mol, gives an extrapolated relative energy of -45.9 kcal/mol. Applying the core-correlation correction of -1.8 kcal/mol yields a best estimate for the energy of ²A₁ Y(HCCH) of -47.7 kcal/mol. In all cases, the raw energies reveal strongly convergent behavior, which was exploited to determine the CBS values listed in Table 5.

The poor convergence of the relative energies is likely a consequence of basis set superposition error (BSSE). We used the counterpoise (CP) method³⁸ to estimate the extent of BSSE. Table 5 reports, in parentheses, the CP-corrected energies for the Y(HCCH) complexes. As expected, the CP corrections diminish from 1.6–1.9 kcal/mol at the aVDZ level to 0.2 kcal/mol at the aVQZ level. The corrected energies reveal convergence that is not apparent in the uncorrected energies. Figure 12 shows the convergence of the ²A₁ values. Extrapolating the CP-corrected relative energies yields a CBS energy of -45.9 kcal/mol, a value identical to that obtained from extrapolating the raw energies. For each of the Y(HCCH) complexes, we find that extrapolating the raw and CP-corrected relative energies yield essentially identical CBS values. Similar behavior is expected for the other structures examined in this work, but was not explored more fully.

References and Notes

- (1) Frenking, G. *Chem. Phys. Lett.* **1983**, *100*, 484.
- (2) Chandrasekhar, J.; Kahn, R. A.; Schleyer, P. v. R. *Chem. Phys. Lett.* **1982**, *85*, 493.
- (3) (a) Chang, N.; Shen, M.; Yu, C. *J. Chem. Phys.* **1997**, *106*, 3237. (b) Chen, W.-C.; Yu, C. *Chem. Phys. Lett.* **1997**, *277*, 245.
- (4) Peterson, K. A.; Dunning, T. H., Jr. *J. Chem. Phys.* **1997**, *106*, 4119.
- (5) (a) Bruce, M. I. *Chem. Rev.* **1991**, *91*, 197. (b) Werner, H. *Angew. Chem., Int. Ed. Engl.* **1990**, *29*, 1077.
- (6) Trenary, M.; Casida, M. E.; Brooks, B. R.; Schaefer, H. F., III. *J. Am. Chem. Soc.* **1979**, *101*, 1638.
- (7) Wakatsuki, Y.; Koga, N.; Yamazaki, H.; Morokuma, K. *J. Am. Chem. Soc.* **1994**, *116*, 8105.
- (8) Wakatsuki, Y.; Koga, N.; Werner, H.; Morokuma, K. *J. Am. Chem. Soc.* **1997**, *119*, 360.
- (9) Silvestre, J.; Hoffman, R. *Helv. Chim. Acta* **1985**, *68*, 1461.
- (10) Sakai, S.; Morokuma, K. *J. Phys. Chem.* **1987**, *91*, 3661.
- (11) Stegmann, R.; Frenking, G. *Organometallics* **1998**, *17*, 2089.
- (12) Nesmeyanov, A. N.; Aleksandrov, G. G.; Antonova, A. B.; Anisimov, K. N.; Kolobova, N. E.; Struchkov, Y.-T. *J. Organomet. Chem.* **1976**, *110*, C36.
- (13) Kasai, P. H. *J. Phys. Chem.* **1982**, *86*, 4092.
- (14) Kasai, P. H. *J. Am. Chem. Soc.* **1992**, *114*, 3299.
- (15) Miralles-Sabater, J.; Merchan, M.; Nebot-Gil, I. *Chem. Phys. Lett.* **1987**, *142*, 136.
- (16) Xie, Y.; Yates, B. F.; Schaefer, H. F., III. *J. Am. Chem. Soc.* **1990**, *112*, 517.
- (17) Tse, J. *J. Am. Chem. Soc.* **1990**, *112*, 5060.
- (18) Cramer, C. J. *J. Mol. Struct. (THEOCHEM)* **1991**, *235*, 243.
- (19) Mele, F.; Russo, N.; Rubio, J.; Toscano, M. *J. Mol. Struct. (THEOCHEM)* **1999**, *446*, 77.
- (20) Scheiner, A. C.; Schaefer, H. F., III. *J. Am. Chem. Soc.* **1985**, *107*, 4451.
- (21) Flores, J. R.; Largo, A. *J. Phys. Chem.* **1992**, *96*, 3015.
- (22) Kasai, P. H.; McLeod, D., Jr.; Watanbe, T. *J. Am. Chem. Soc.* **1977**, *99*, 3521.
- (23) Kasai, P. H. *J. Am. Chem. Soc.* **1982**, *104*, 1165.
- (24) Stauffer, H. U.; Hinrichs, R. Z.; Willis, P. A.; Davis, H. F. *J. Chem. Phys.* **1999**, *111*, 4101.
- (25) Siegbahn, P. E. M. *Theor. Chim. Acta* **1994**, *87*, 277.
- (26) (a) Becke, A. D. *J. Chem. Phys.* **1993**, *98*, 5648. (b) Lee, C.; Yang, W.; Parr, R. G. *Phys. Rev. B* **1988**, *37*, 785.
- (27) (a) Dunning, T. H., Jr. *J. Chem. Phys.* **1989**, *90*, 1007. (b) Kendall, R. A.; Dunning, T. H., Jr.; Harrison, R. J. *J. Chem. Phys.* **1992**, *96*, 6796. (c) Woon, D. E.; Dunning, T. H., Jr. *J. Chem. Phys.* **1993**, *98*, 1358.
- (28) Andrae, D.; Haeussermann, U.; Dolg, M.; Stoll, H.; Preuss, H. *Theor. Chim. Acta* **1990**, *77*, 123.
- (29) Peterson, K. A. Private communication.
- (30) Frisch, M. J.; Trucks, G. W.; Schlegel, H. B.; Scuseria, G. E.; Robb, M. A.; Cheeseman, J. R.; Zakrzewski, V. G.; Montgomery, J. A., Jr.; Stratmann, R. E.; Burant, J. C.; Dapprich, S.; Millam, J. M.; Daniels, A. D.; Kudin, K. N.; Strain, M. C.; Farkas, O.; Tomasi, J.; Barone, V.; Cossi, M.; Cammi, R.; Mennucci, B.; Pomelli, C.; Adamo, C.; Clifford, S.; Ochterski, J.; Petersson, G. A.; Ayala, P. Y.; Cui, Q.; Morokuma, K.; Malick, D. K.; Rabuck, A. D.; Raghavachari, K.; Foresman, J. B.; Cioslowski, J.; Ortiz, J. V.; Baboul, A. G.; Stefanov, B. B.; Liu, G.; Liashenko, A.; Piskorz, P.; Komaromi, I.; Gomperts, R.; Martin, R. L.; Fox, D. J.; Keith, T.; Al-Laham, M. A.; Peng, C. Y.; Nanayakkara, A.; Gonzalez, C.; Challacombe, M.; Gill, P. M. W.; Johnson, B.; Chen, W.; Wong, M. W.; Andres, J. L.; Gonzalez, C.; Head-Gordon, M.; Replogle, E. S.; Pople, J. A. *Gaussian 98*, Revision A.7; Gaussian, Inc.: Pittsburgh, PA, 1998.
- (31) (a) Peterson, K. A.; Woon, D. E.; Dunning, T. H., Jr. *J. Chem. Phys.* **1994**, *100*, 7410. (b) Woon, D. E.; Dunning, T. H., Jr. *J. Chem. Phys.* **1994**, *101*, 8877.
- (32) (a) MOLPRO is a package of ab initio programs written by H.-J. Werner and P. J. Knowles with contributions from J. Almlof, R. D. Amos, A. Berning, D. L. Cooper, M. J. O. Deegan, A. J. Dobbyln, F. Eckert, S. T. Elbert, C. Hampel, R. Lindh, A. W. Lloyd, W. Meyer, A. Nicklass, K. Peterson, R. Pitzer, A. J. Stone, P. R. Taylor, M. E. Mura, P. Pulay, M. Schutz, H. Stoll, and T. Thorsteinsson. (b) Hampel, C.; Peterson, K.; Werner, H.-J. *Chem. Phys. Lett.* **1992**, *190*, 1. (c) Knowles, P. J.; Hampel, C.; Werner, H.-J. *J. Chem. Phys.* **1993**, *99*, 5219.
- (33) Glendening, E. D.; Badenhoop, J. K.; Reed, A. E.; Carpenter, J. E.; Bohmann, J. A.; Morales, C. M.; Weinhold, F. *NBO 5.0*; Theoretical Chemistry Institute: University of Wisconsin, Madison, WI, 2001.
- (34) Nguyen, M. T. *J. Phys. Chem.* **1988**, *92*, 1426.
- (35) Burnett, S. M.; Stevens, A. E.; Feigerle, C. S.; Lineberger, W. C. *Chem. Phys. Lett.* **1983**, *100*, 124.
- (36) Jensen, M. J.; Pedersen, U. V.; Andersen, L. H. *Phys. Rev. Lett.* **2000**, *84*, 1128.
- (37) We use an unrestricted “different Lewis structures for different spins” description of the open-shell systems in this study. The lines and dots of these “spin-Lewis structures” respectively represent *single* bonding and nonbonding electrons of the α and β manifolds. The α and β Lewis structures together describe the hybridization and bonding character of the complex. When the α and β Lewis structures exhibit the same bonding pattern, we collapse the two into a standard “restricted” Lewis structure in which the lines represent doubly occupied bonds.
- (38) Boys, S. F.; Bernardi, F. *Mol. Phys.* **1970**, *19*, 553.